Sensors & Actuators: B. Chemical 334 (2021) 129599

Contents lists available at ScienceDirect

Sensors and Actuators: B. Chemical

journal homepage: www.elsevier.com/locate/snb

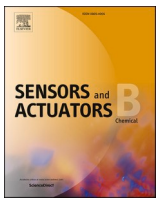

A novel multi-frequency trans-endothelial electrical resistance (MTEER) sensor array to monitor blood-brain barrier integrity

Maider Badiola-Mateos [a,b,1], Davide Di Giuseppe [e,f,1], Roberto Paoli [a,b,1], Maria Jose Lopez-Martinez [a,b,c], Arianna Mencattini [e,f], Josep Samitier [a,b,c,d,**], Eugenio Martinelli [e,f,*]

[a] Nanobioengineering Group, Institute for Bioengineering of Catalonia (IBEC) Barcelona Institute of Science and Technology (BIST), 12 Baldiri Reixac 15-21, Barcelona 08028, Spain
[b] Department of Electronics and Biomedical Engineering, University of Barcelona, Martí i Franquès 1, 08028 Barcelona, Spain
[c] Centro de Investigación Biomédica en Red en Bioingeniería, Biomateriales y Nanomedicina (CIBER-BBN), Monforte de Lemos 3-5, Pabellón 11, 28029 Madrid, Spain
[d] Institute of Nanoscience and Nanotechnology, Universitat de Barcelona (UB), 08028 Barcelona, Spain
[e] Department of Electronic Engineering, University of Rome Tor Vergata, Via del Politecnico 1, 00133 Rome, Italy
[f] Interdisciplinary Center for Advanced Studies on Lab-on-Chip and Organ-on-chip Applications (IC-LOC), University of Rome Tor Vergata, Via Montpellier 1, 00133 Rome, Italy

ARTICLE INFO

Keywords:
Electrical impedance spectroscopy
Microelectrodes
Impedance sensors
MTEER
Rapid prototyping
Machine learning
Blood-Brain barrier
Cellular barrier integrity monitoring

ABSTRACT

The blood-brain barrier (BBB) is a dynamic cellular barrier that regulates brain nutrient supply, waste efflux, and paracellular diffusion through specialized junctional complexes. Finding a system to mimic and monitor BBB integrity (i.e., to be able to assess the effect of certain compounds on opening or closing the barrier) is of vital importance in several pathologies. This work aims to overcome some limitations of current barrier integrity measuring techniques thanks to a multi-layer microfluidic platform with integrated electrodes and Multi-frequency Trans-Endothelial Electrical Resistance (MTEER) in synergy with machine learning algorithms. MTEER measurements are performed across the barrier in a range of frequencies up to 10 MHz highlighting the presence of information on different frequency ranges. Results show that the proposed platform can detect barrier formation, opening, and regeneration afterwards, correlating with the results obtained from immuno-staining of junctional complexes. This model presents novel techniques for a future biological barrier in-vitro studies that could potentially help on elucidating barrier opening or sealing on treatments with different drugs.

1. Introduction

The blood-brain barrier (BBB) is one of the challenging scenarios where Lab on chip (LoC) devices can be applied through a synergic integration of chemical sensors, multi-electrode measurement devices, and microscopy techniques, and more recently, deep learning techniques [1].

The BBB is a dynamic biological barrier that is localized at the central nervous system (CNS) microvessels. It is responsible for mediating brain supply of nutrients, waste efflux and inhibiting paracellular diffusion, forcing the transport of each kind of molecule through different transcellular mechanisms [2]. In this way, it protects the CNS from: toxins, ion fluctuations (that would otherwise affect synaptic and axonal signaling), interferences with neurotransmitters released in the peripheral nervous system, inflammation, and macromolecules [3]. The BBB permeability is controlled by the junctional complexes: tight junctions (TJ), adherens junctions (AJ), and gap junctions [4,5]. Those complexes are intertwined nets of proteins that have a role in controlling the passage of substances. The major transmembrane AJ protein is vascular endothelial cadherin (VE-cadherin) [6]. VE-cadherin based AJ are regulated by zonula occludens 1 (ZO-1), one of the main components of the TJ, essential for an efficient endothelial barrier formation [7].

* Corresponding author at: Department of Electronic Engineering, University of Rome Tor Vergata, Via del Politecnico 1, 00133 Rome, Italy.
** Corresponding author at: Nanobioengineering group, Institute for Bioengineering of Catalonia (IBEC) Barcelona Institute of Science and Technology (BIST), 12 Baldiri Reixac 15-21, Barcelona 08028, Spain.
E-mail addresses: jsamitier@ibecbarcelona.eu (J. Samitier), martinelli@ing.uniroma2.it (E. Martinelli).
[1] These authors contributed equally to this work.

https://doi.org/10.1016/j.snb.2021.129599
Received 26 October 2020; Received in revised form 27 January 2021; Accepted 30 January 2021
Available online 8 February 2021

Modulating the barrier tightness by opening it for drug delivery to the CNS (for cancer or neurological disease treatment) or closing it for pathologies involving BBB dysfunction and leakiness (such as stroke, Alzheimer or multiple sclerosis, among others [2,4]), is still a challenge. There are two gold standard techniques to monitor the membrane integrity: quantification of the diffusion of different tracers by fluorescence or luminescence quantification and trans-epithelial electrical resistance (TEER) measurements.

Tracer diffusion permeability assays measure the diffusion of a known tagged compound from a donor to a receiver compartment and facilitate determining the size and charge selectivity of the membrane [8]. Although it is low-cost and it helps assessing transepithelial transport in both directions, this method has three main drawbacks: the tracers have to be carefully chosen not to interfere with the BBB function or the experiment; each tracer provides discrete limited information about the specific tracer-related membrane pore size and charge instead of global membrane integrity; and it is a single time-point analysis. On the other hand, TEER measurement can detect the cell differentiation and quantify the net movement of ions across the barrier and it can be performed in real-time without damaging cells [9–13]. However, this technique has some major limitations: a complex biological process, such as BBB permeability variations, is resumed in a single numeric value that depends also on the electrode properties and positioning. Also, the TEER gives only an overall information on the barrier tightness and often may occur that changes of the barrier permeability on specific compounds are not reflected in changes of the barrier resistance and vice versa [14].

Microfluidic LoC devices offer the advantage of mimicking biological barriers in compartmentalized systems [15,16] while integrating electrodes for performing electrical measurements on a biological microenvironment [17–19].

In this work, we have developed a LoC made of Cyclic-Olefin Polymer (COP) with small feature size electrodes directly integrated on the device surface that enables to perform Electric Impedance Spectroscopy (EIS) measurements in multiple positions. Through the synergy of multiband frequency measurement techniques, and machine learning algorithms we developed a non-invasive method for real time monitoring of the BBB integrity. In order to test this platform, we selected a simplified and well-assessed BBB *in-vitro* model of endothelial cells and pericytes that were cultured inside the microfluidic device. We induced the barrier degradation with mannitol drug and we monitored the barrier integrity evolution from its formation though the disruption to the recovery by measuring in real time the barrier impedance in a frequency range from 100 Hz to 10 MHz.

The novelty of the proposed approach relies to the capability of analyzing the multi-band impedance measurement across multiple positions using pattern recognition and machine learning algorithms to obtain a multivariate representation of trans-endothelial electrical resistance (MTEER), providing a tool for on-line barrier tightness monitoring that is complementary to the tracer diffusion measurements for molecular permeability.

The originalities of this work regard multiple aspects; with respect to the measurement technique, the use of the impedance spectrum has been exploited to enlarge the capability provided by TEER to a wider range of frequencies for maximizing the amount of information that can be acquired from the electric measurements [13,20]. In fact, most of the commercial instruments dedicated to TEER, work in a limited impedance range with a claimed resistance accuracy of 0.1 % [21]. Recent works show that the use of chopstick electrodes generates a non-uniform current density across the cell layer and this may affect the measurement repeatability due to the electrode positioning [22]. In addition, the high cell resistance at the low working frequencies of these devices (~12.5 Hz) may result in very low measured currents that are more affected by noise [9,22]. As a direct consequence, for this work, we used precision impedance analyzers that guarantee a better accuracy over a much wider impedance and frequency range. Also, we designed specific electrodes that limit some parasitic effects that may occur during the measurements. To this aim, we kept the distance between the electrodes and the instrument probes as short as possible to limit the series inductance and resistance and we routed the traces on the top layer perpendicularly to the ones on the bottom to reduce the stray capacitance on the chip substrate. These necessities leaded to the use of COP as a substrate for the electrodes since it has been demonstrated to be non-toxic for the cells, to have enough high glass transition temperature to allow the deposition of metals by sputtering, a better oxygen permeability with respect to other hard polymers [23] and an excellent optical clearance, suitable for optical inspection [24].

Regarding the material used to fabricate the LoC device, the use of hard polymers allowed to exploit some rapid-prototyping techniques such as laser cutting [25] that enabled the massive fabrication of multilayer devices. This provided a high flexibility in the design and testing using CAD tools, but it also enabled the integration of more substrate materials in a single microfluidic device to exploit the most useful properties of each material. In fact, the fabricated device uses Poly-methyl meta-acrilate (PMMA) as a hard base to avoid deformations in the bonding process, several thin COP layers forming the channel structures, polycarbonate (PC) for the porous membrane, gold for the electrodes and medical grade silicon based transfer tape to perform the bonding.

With respect to the experimental set-up and chip production, the chip layout has been designed in order to have multiple replicas of the BBB structure in the same chip, with a total of 16 testing points that run in parallel to maximize the throughput of a single cell seeding [26].

A simplified BBB model was replicated in the microfluidic devices (μBBB) that includes both endothelial cells (ECs) and pericytes, which have been demonstrated to be relevant for the AJ/TJ formation [27,28].

Moreover, in some 3D vessel-like structures of ECs [29], the use of TEER or EIS measurements to monitor the barrier function can be very tricky for placing electrodes on opposite sides of the functional EC structure. To minimize the electrical measurement difficulties, we fabricated a BBB functional unit formed by a PC membrane that acts as a scaffold for the ECs and pericytes. This ensures a better cell adhesion, the possibility to perfuse medium at higher flowrates and an easier electrical probing.

Finally, but not less relevant, in virtue of the multidisciplinary synergy of this work, the MTEER measurements were analyzed using machine learning algorithms trained and tested on a high number of independent measurements acquired in distinct locations.

2. Experimental

2.1. Device fabrication

The device was designed in Autodesk Inventor® (see Fig. 1), and it consists of a PC transparent membrane (Model 9100−4710, pore size 1 μm, thickness 10 μm, Whatman®, Sigma-Aldrich). This membrane is sandwiched between two COP layers patterned with networks of 4 parallel microfluidic channels (2 mm width, 180 μm height, 20 mm length). Microchannels in one layer were place perpendicular from one layer to the other, generating 16 intersections.

An array of concentric interdigitated electrodes is fabricated on top of additional COP layers (Zeonor® 1420R, Zeon Corporation, Tokyo, Japan). Each channel intersection features two pairs of electrodes, one on the roof of the upper channel and one on the floor of the bottom channel (Fig. 1). Electrodes are routed to contact pads on two opposite external flaps which protrude from the final assembly and are sized according to industry standard Zero Insertion Force (ZIF) connectors (model 52271−1679, Molex, US).

Initially, 180 μm thick COP substrate is rinsed in 2-propanol (IPA, Sigma-Aldrich, 278475) and dried using N_2 gas stream. A silicone double sided biocompatible pressure sensitive adhesive (PSA, ARSeal® 8026, Adhesive Research, Inc., US) was chosen to glue the different COP

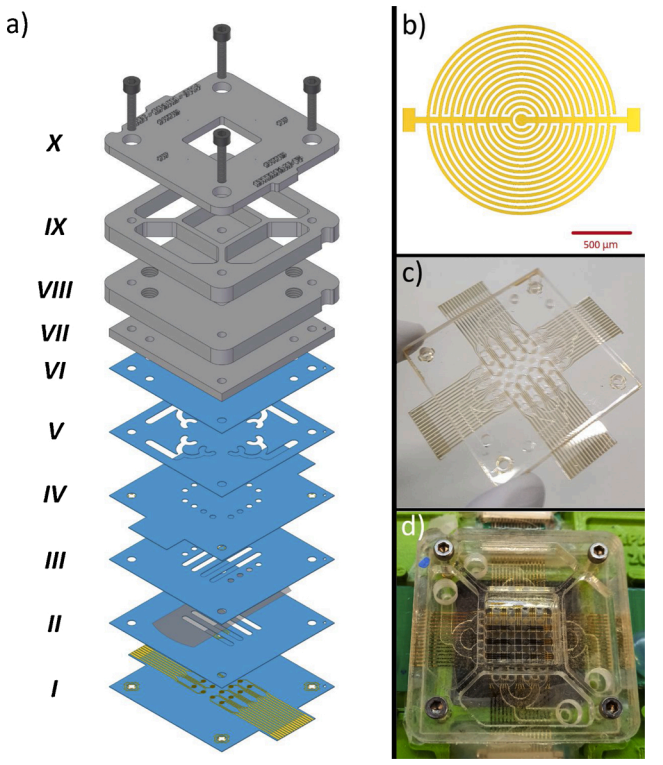

Fig. 1. a) Exploded diagram of the device: I base laser with bottom-side electrodes, II bottom-side channels with on top the porous PC membrane (grey color), III top-side channels, IV top-side electrodes (facing downwards), V fluid splitter, VI top layer, VII mini-Luer interface layer, VIII ¼-28 UNF threaded interface layer, IX medium tank, X cover slip; the layers in blue are made of COP and the ones in gray are made of PMMA. b) Detail of the interdigitated electrodes design, the fingers feature size is 50 µm. c) Picture of the fabricated device without the PMMA medium tank. d) Picture of the fabricated device placed inside its holder in operative condition (For interpretation of the references to colour in this figure legend, the reader is referred to the web version of this article).

layers and the membrane, for its biocompatility very low thickness and its formulation with polyester release liners, which is compatible with laser processing. This adhesive is laminated on the substrate, avoiding bubble formations. PMMA was the material preferred for the interfacing layers for its cleaner cuts in thicker substrates when processed with CO_2 laser. 467 M P transfer tape (3M™ Maplewood, US) was laminated onto PMMA sheets (thickness of 3 and 6 mm) before cutting. A Trotec Speedy 100 laser cutter (Trotec Laser Inc., Austria) was used cut all the layers. To simplify user handling and improve versatility, each of the four microfluidic ports included two type of standard microfluidics connectors (Mini-Luer® and ¼-28 Unified National Fine thread) and a medium reservoir (volume: 2 mL) fabricated in PMMA. Before assembly, gold electrodes were fabricated on top of new COP layers. After sputtering the substrates with 100 nm of gold, a 2 µm thick layer of AZ® 5214-E photoresist (AZ® 5214-E, AZ® 400 K Developer and AZ® 100 Remover, Microchemicals GmbH, Germany) is spun on the substrate (2000 rpm, 30 s) and baked at 95 °C on a hotplate. The substrate was aligned with a chrome mask, exposed with UV light (Energy 200 mJ cm^{-2}) and developed for 30 s using 1:4 dilution of AZ® 400 K Developer in milli-Q water. Gold was wet etched using TFA etchant (Transene Co Inc., US) for 40 s. Finally, the photoresist was removed by washing in AZ® 100 Remover for 60 s. The membrane was manually cut to size using a template and positioned in contact with the channels.

Assembly was performed with the help of a custom-made aluminum aligner consisting of a base (70 × 70 × 10 mm) with 4 press-fitted steel dowel pins and a cover with 4 holes (70 × 70 × 10 mm). Each layer design included 4 alignment holes at the corners, matching the corresponding dowel pin for accurate alignment. The device was finally obtained by pressing together the layers on a hydraulic press (BETA 3027 10, Italy) at 120 bar.

2.2. On-chip cell culture

Each device was activated using UVO_3 tip cleaner (BioForce, US) for 20 min under a fume hood and interfaced with Tygon® tubing to a PHD 2000 Syringe Pump (Harvard Apparatus, US). After sterilization with EtOH 70 % solution (2 mL), the devices were washed twice with sterile PBS (2 mL). Upper and lower channel were coated using gelatin (2 mg mL^{-1}) and Collagen type-I (1:20) in sterile PBS, respectively (see Supplementary Information for the technical details).

Cell seeding was performed starting from lower channel. hCMEC/D3 cells were trypsinized using trypsin-EDTA and resuspended in EC culture medium: EndoGRO MV complete culture medium supplemented with 1 ng mL^{-1} basic fibroblast growth factor (bFGF) and 1% penicillin-streptomycin (P/S)). The inlet reservoir was filled with 500 µL hCMEC/D3 cell suspension ($2.8{\cdot}10^6$ cells mL^{-1}) and 200 µL were perfused through the lower channel (flowrate: 50 µL min^{-1}). The device was then flipped upside-down and incubated at 37 °C for 2−3 h to promote EC attachment onto the membrane. Bovine pericytes [30] were trypsinized using trypsin-EDTA, resuspended in pericyte culture medium (DMEM supplemented with 20 % calf serum, 1 ng mL^{-1} bFGF and 1% P/S) and seeded in the upper channel at $2{\cdot}10^6$ cells mL^{-1}, leaving the devices afterwards incubating upwards for at least 2 h at 37 °C. After verifying cell adhesion, 1 mL of medium was perfused through each channel (flowrate: 50 µL min^{-1}). Devices were incubated in a humidified CO_2 incubator at 37 °C, with reservoirs filled of corresponding media and covered with a lid, changing the media every day applying flow (flowrate of 50 µL min^{-1} for the devices). At DoC+2, 48 h after confluency was reached, experimental samples (µBBB devices) were treated with D-Mannitol (0.3 M, 45 min, 37 °C), and then washed and changed back to their supplemented culture medium, whereas control devices (µBBB controls) were fixed. At DoC+3, µBBB devices were also fixed.

As experimental controls of the compartmentalized device coculture, hCMEC/D3 (50.000 cell cm^{-2}) and pericytes (36.000 cell cm^{-2}) were seeded independently in Petri dishes following the same procedures. In all cases, the medium was changed daily. Some of these Petri dish controls were also treated with mannitol in the same way at DoC+2 and fixed at DoC+2 (right after mannitol treatment) and at DoC+3. Non treated Petri dish controls were fixed at DoC+3. The cell fixation was performed incubating samples in a 4% paraformaldehyde solution for 30 min at room temperature, or in the case of microdevices, flowing the solution through the channels, then washed and stored at 4 °C in PBS solution with 0.02 % of sodium azide.

2.3. Immunostaining

All the following steps were performed at room temperature (unless stated otherwise), using a negative flowrate of 50 µL min^{-1}, after aspirating and replacing the liquid in the inlet reservoir at each step. Volumes indicated below are referred to the quantity flowed through each channel. Devices were washed twice with 0.75 mL of PBS 1 × . Cell membranes were permeabilized with 1 mL of PBS-triton 0.1 % solution. Then blocking solution (0.5 mL, PBS with 0.1 % Triton and 10 % FBS) is flowed and left in incubation for 2 h. Channels were washed flowing PBS-triton 0.1 % solution (1 mL). Primary antibody solution (0.5 mL, rabbit polyclonal anti-VE-cadherin antibody, 1:1000) was perfused through each channel and left in incubation overnight at 4 °C. Channels were washed again with PBS-triton 0.1 % solution (1.5 mL) before applying secondary antibody solution A (0.5 mL, 1 h incubation, Alexa Fluor 568 goat anti-rabbit, 1:1000). From that point, devices were kept protected from light. Devices were washed again with PBS-triton 0.1 % and secondary antibody solution is applied (0.5 mL, 3 h incubation,

Alexa Fluor 488 ZO-1 monoclonal antibody, 1:100). Channels were washed again using PBS 1X (1.25 mL) before applying Hoechst-PBS solution (0.5 mL, 32.4 μM of Hoechst 33342, 10 min incubation) and finally washed with PBS-azide (1.5 mL, 0.02 %). Fluorescence imaging was performed using an inverted confocal Leica SP5 microscope. Afterwards, images were processed with ImageJ software.

2.4. MTEER measurements

A custom interface was designed in AutoDesk Inventor® and 3D-printed using Poly-lactic acid (PLA) (0.3 mm layer thickness), to fix the LOC inside a digital O_2/CO_2 and temperature controlled H301 mini-incubator (Okolab srl, Italy). This interface houses four Bartels MP6-pp piezoelectric micropumps (Bartels Mikrotechnik GmbH, Germany) that allow the online change of medium, provides an electromagnetic shielding for the noise measurements reduction and a waterproof sealing to avoid the formation of moisture on the ohmic contacts of the chip. The incubator was maintained at 37 °C, 97 % Humidity, 5% CO_2, 10 % O_2 during all the measurements. Culture media change was performed daily by replacing media in the reservoir and flowing 1 mL through the channels (flowrate: 50 μL· min^{-1}). After media change, inlet reservoirs were covered to prevent evaporation and the temperature was left stabilizing before starting the measurements. Impedance spectroscopy measurements were performed by using an Agilent 4294A Precision Impedance Analyzer (Agilent, US). The interface was connected to the instrument in a shielded two terminal configuration [31].

This configuration employs two coaxial cables (see Supplementary Information Fig. S5) to reduce the effects of stray capacitance between the leads, extending the typical impedance range above 100 kΩ. The outer shielding of the coaxial cables is connected to the guard terminal and to the guard electrodes.

3. Results

3.1. Device functionality

A novel *in-vitro* microfluidic platform (Fig. 1) was designed and fabricated to perform impedance spectroscopy measurements across a tissue-tissue interface, obtained by co-culture of two different types of cells. This device (μBBB device), consists of two networks of 4 parallel microfluidic channels cut through COP sheets and separated by a porous polycarbonate membrane. The two microchannel networks are intersecting perpendicularly, forming 16 intersections (surface area: 4 mm^2 each) in a single device. Each intersection forms a structure as shown in Fig. 2, including two pairs of interdigitated electrodes that are located on the top of the upper channel and on the bottom of the lower channel. This structure accommodates the membrane in the middle. This design was chosen to increase total contact surface between the two cell cultures and enables impedance spectroscopy measurements in multiple independent positions across the device, in real-time, to maximize the throughput on a single experiment. The fabrication process is very rapid and accurate since it exploits laser cutting, in fact, a complete device can be cut and be fully assembled in less than 10 min.

3.2. Assessment of junctional complexes

An *in-vitro* model of the BBB was made seeding brain endothelial cells hCMEC/D3 together with pericytes cultured on opposite sides of a membrane. Cells were exposed to shear stress through media change every 24 h. The experiment time-points were normalized in reference to the moment when around 90 % of cell coverage was reached on the layer (DoC, day of confluency). 48 h after reaching the confluency (DoC+2), experimental devices ("μBBB-treated") were exposed to mannitol and fixed 24 h later (DoC+3), while control devices ("μBBB-controls") were fixed without being treated (DoC+2). The comparison between samples led to observe alterations in junctional complexes. The effect of mannitol onto EC and pericytes independently (seeded on Petri dishes) was also analyzed (Supplementary Information Fig. S1 and Fig. S2).

We compare the expression of relevant TJ and AJ markers related to confluency in μBBB devices when samples were not treated and when they were treated with mannitol and left for 24 h recovery (Fig. 3). Two different positions on the device where selected for the evaluation of mannitol effect.

At the bottom-position of the device, where EC were not in close contact with pericytes, ZO-1 signal was detected in the cytoplasm and VE-cadherin in the cell periphery (Fig. 3, a and b). But after mannitol treatment and 24 h recovery, ZO-1 expression was reduced to cytoplasmatic and nuclear localization, and VE-cadherin was severely affected and vanished, related with the high apoptosis levels (as observed with the nuclear staining) (Fig. 3, c and d).

At the membrane-position of the device, where both EC and pericytes were interacting at each side of the membrane, ZO-1 signal was detected predominantly in cell nuclei and some small areas of cell-membrane, and VE-cadherin expression was almost absent (Fig. 3, e and f). After mannitol treatment and 24 h recovery, ZO-1 signal decreased slightly and remained exclusively with nuclear and cytoplasmic localization, whereas VE-cadherin staining remained the same, almost absent, and confluency decreased slightly (Fig. 3, g and h).

Moreover, a fluorescent tracer permeability test has been conducted on the μBBB-treated devices (see Supplementary Information, Fig. S4) showing a net difference in terms of tracer diffusion between the formed membrane and the membrane damaged by mannitol treatment.

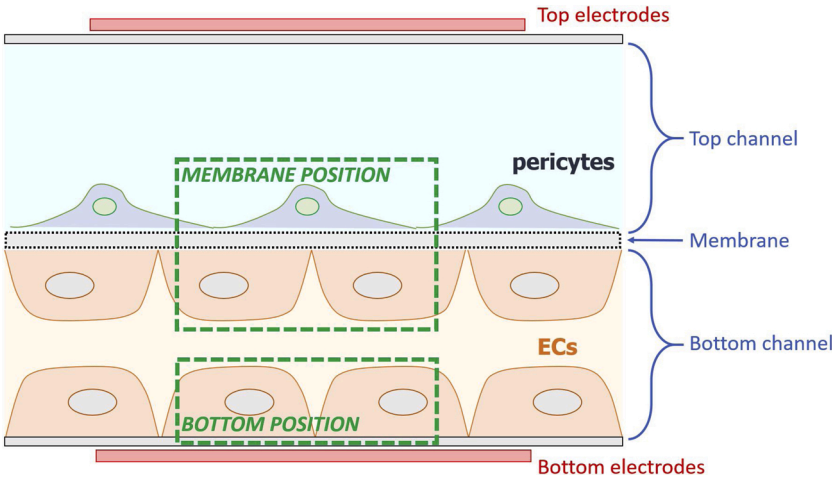

Fig. 2. Functional structure of each intersection on the "μBBB device". Endothelial cells (ECs) are seeded in the bottom channel in contact with the bottom of the device and with the PC membrane, while pericytes are seeded on the bottom of the upper channel in contact with the PC membrane. Both membrane-position and bottom-position are analyzed later on for imaging purposes. Each channel is covered with the culture medium required for each cell type. A pair of interdigitated electrodes is located on the top of the upper channel and on the bottom of the lower channel to perform MTEER measurements.

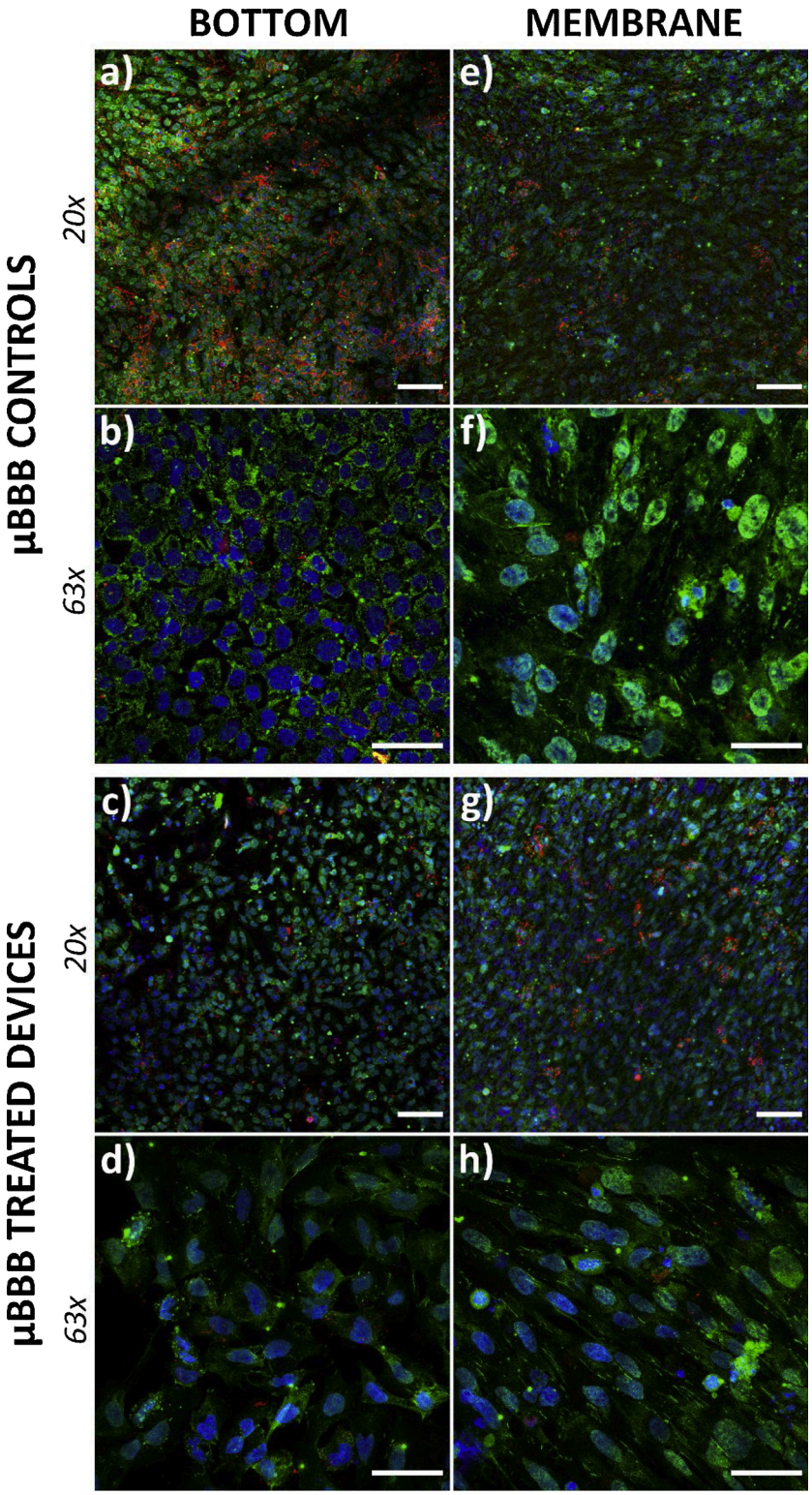

Fig. 3. Immunostaining of μBBB-controls, non-treated, DoC+2 (a, b, e, f) and μBBB-treated devices, 24 h after the exposure to mannitol treatment, DoC+3 (c, d, g, h). Confocal microscopy images show Z-projection of the membrane-position, observing the two cells layers, pericytes and endothelial, (e-h) and bottom-position, observing only endothelial layer, (a-d) for both devices at 20X and 63X augments. ZO-1 tight junctions are stained in green. VE-cadherin adherens junctions are stained in red. Nuclei are stained in blue. Scale bars are 100 μm for 20X images and 50 μm for 63X images (For interpretation of the references to colour in this figure legend, the reader is referred to the web version of this article).

3.3. MTEER results

The goal is to develop a classification model based on the impedance measurements [32], that can recognize the cell status based on training data of selected time-points.

MTEER measurements were performed across the μBBB device membrane in five different intersections, over 5 days after cell seeding. Each intersection was considered a different sample under the same experimental conditions since there were small variations among positions in terms of the cell number, tolerance on the alignment of the electrodes, etc. From DoC-1 to DoC+3 included, 100 spectra were acquired every 24 h on each position through an automated software written in MATLAB R2019a environment (MathWorks, US). Each spectrum was acquired in a frequency range between 100 Hz and 10 MHz, spanning 300 points in a logarithmic scaling as shown in Fig. 4.

The trans-membrane impedance was measured, across a defined

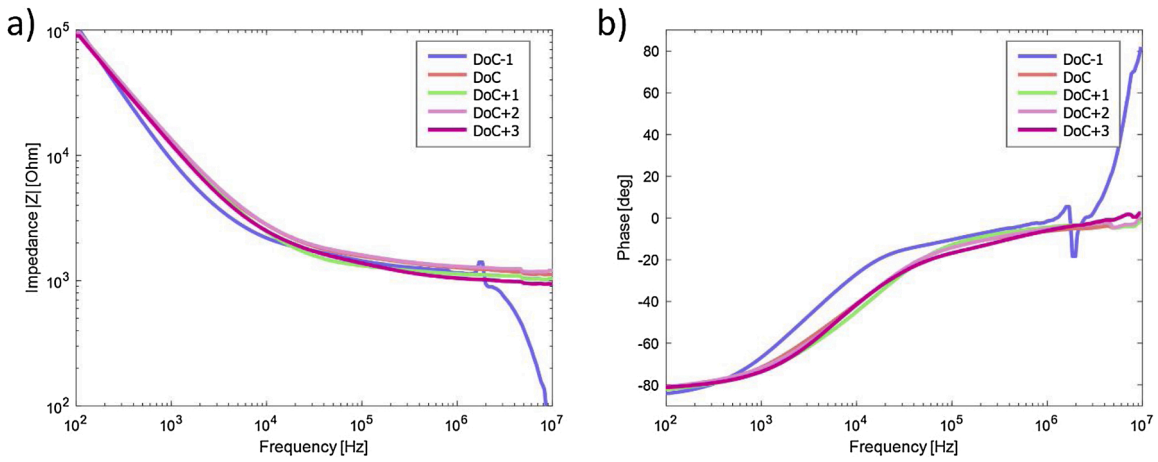

Fig. 4. EIS spectra measurement at a single intersection of μBBB device. Each colored line represents each experimental time-point in the same intersection (from DoC-1 to DoC+3). a) impedance modulus spectra and b) impedance phase spectra frequency variations of a given intersection of the device.

frequency range, through its modulus |Z| and phase ϕ equations, defined as:

$$|Z|(f) = \sqrt{R(f)^2 + X(f)^2} \tag{1}$$

$$\varphi(f) = \arctan\left(\frac{X(f)}{R(f)}\right) \tag{2}$$

where R is the resistance and X is the reactance at given frequency f.

Impedance measurements repeatability was assessed by quantifying the coefficient of variation among different measurement results, defined as:

$$Fluctuation(f)[\%] = \frac{\sigma(f)}{\mu(f)} * 100 \tag{3}$$

where σ and μ are respectively the standard deviation and the mean value of the spectrum at given frequency across all the measurements done at a specific time-point and in a specific intersection of the device. It resulted in a 2.5 % of maximum fluctuation across all the datasets.

The acquired measurements were divided in two distinct datasets, one for the impedance modulus data and the other for the phase. Each of them consisted of 2500 total measurements by 300 spectral-line features matrix. The data analysis was performed in MATLAB environment using a classification toolbox [33].

A preliminary analysis was first conducted for both impedance modulus and phase datasets, using an LDA (Linear Discriminant Analysis) classifier.

For the impedance modulus dataset, an LDA model has been trained with the measurements of 3 of intersections (1500 measurements) and tested with the data of the remaining 2 intersections (1000 measurements). A 5 groups venetian-blinds cross-validation was used and resulted in 97 % accuracy in training. The accuracy in testing dropped to 85 % due to misclassification of the samples belonging to the classes DoC and DoC+3.

A further LDA model was trained with impedance phase data and choosing the same intersections for training and testing as for the previous model. It resulted a 100 % accuracy in training and in test.

To better understand the misclassification issues on the impedance modulus dataset, a forward sequential feature selection (SFS) was performed using LDA criterion, with random training and testing subsets in a proportion of 60 % for training and 40 % for testing of the total dataset. After 100 iterations, as shown in Fig. 6, the SFS did not select any features in lower frequency band (f < 10 kHz). The same procedure was used also for the phase dataset and resulted that the most selected features were in the same frequency range of the impedance dataset.

The results in Table 1 show the average model accuracy values across all the possible combinations of training and test for each features subset.

Fig. 7 shows the plot of the first two discriminant directions of one of the ten LDA models, considering only the selected features. It resulted in a 100 % accuracy in testing so this model is capable of separating all the classes corresponding to different time-points and therefore it can attribute to each class a biological meaning, despite the separability between the class DoC and DoC+3 was much lower with respect to the other classes.

4. Discussion

The study presented here shows a novel method to monitor barrier integrity that could be used to optimize the *in-vitro* screening of drug administration for neurological diseases where BBB is involved. The potentiality of the proposed platform is based on the combination of *in-vitro* multiple cell-culture in a microfluidic device together with the use of machine learning algorithms to analyze the acquired MTEER data and look for the informative content. In particular, we analyzed the discrimination power of a gold standard classification model as LDA. The first model based on the impedance modulus spectra presented an accuracy of 85 % in testing due to misclassifications of the samples belonging to classes DoC and DoC+3, as shown in the score plot in Fig. 5a. Performing a SFS, it resulted that most informative features lay in the 10 kHz – 10 MHz band. This suggests that the dominant trend in the lower band (see Fig. 4, panel a) is mostly due to the electrode capacitance filtering [34]. Results also showed that the most selected features are common to the two datasets, as shown in Fig. 6 and there are some particular frequencies (10 kHz, 1.07 MHz and 4.81 MHz) that could carry the information of some specific biological processes. In fact,

Table 1
Average model accuracy across 10 combinations of training and testing for several subset of features. The SFS selected features refers to features that are over the threshold of the 10 % of selection.

Frequency range	# features	Accuracy |Z|	Accuracy φ
Full spectrum	300	83,1% (75,1 – 91,1) %	97,1% (92,7 – 100) %
10 kHz – 10MHz	180	85,4% (78,5 – 92,3) %	99,0% (95,8 – 100) %
Selected features on |Z|	9	90,7% (86,1 – 95,3) %	81,2% (71,3 – 91,1) %
Selected features on ϕ	6	83,9% (72,3 – 95,5) %	94,1% (85,9 – 100) %

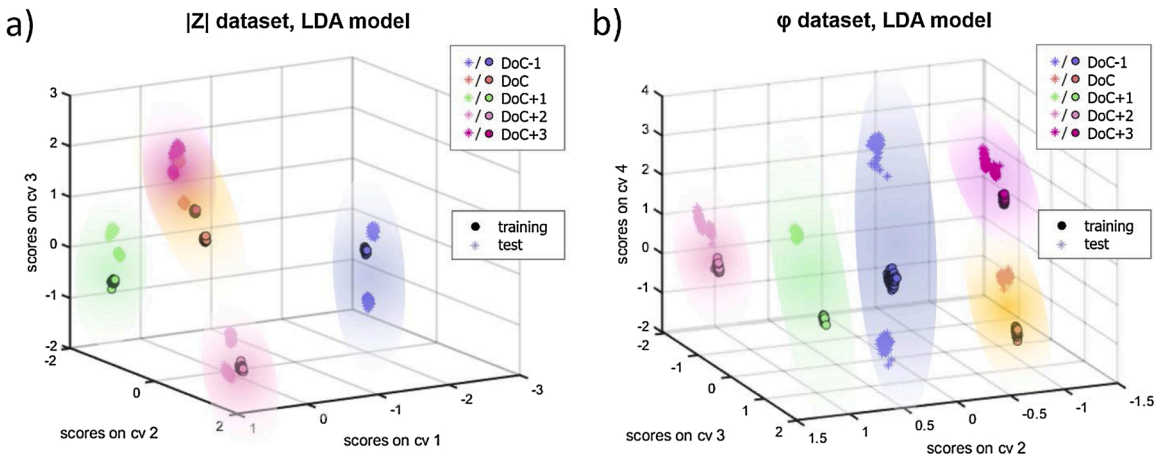

Fig. 5. a) LDA model based on impedance modulus |Z| data acquired between DoC-1 and DoC+3. 3D score plot on canonical variables 1, 2 and 3. Dots represent training data and asterisks the test data. b) LDA model based on impedance phase data φ(Z) acquired between DoC-1 and DoC+3. Plot of scores projection on canonical variables 2, 3 and 4. Dots represent training data, asterisks the test data and the colored area represents the spatial extension for each class.

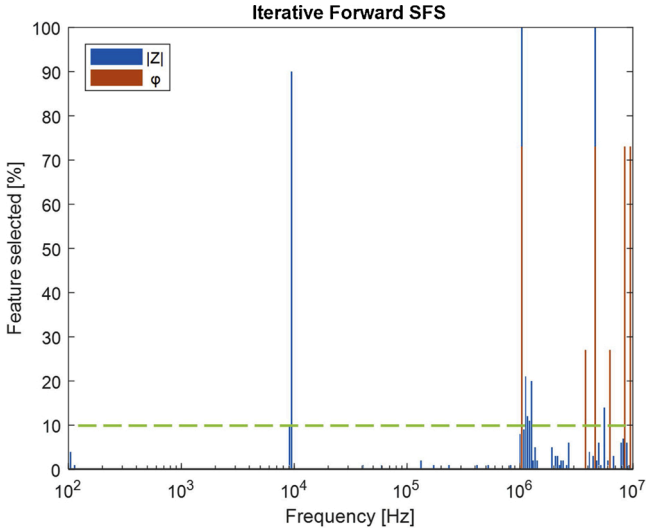

Fig. 6. Bar plot showing the percentage of selection for spectral features; the selected features for the impedance modulus dataset are shown in blue, and the ones for impedance phase dataset are shown in red. The total number of iterations is 100 for each dataset. Subsets of features that have more than 10 % selection percentage (dashed green line) were used to build classification models (For interpretation of the references to colour in this figure legend, the reader is referred to the web version of this article).

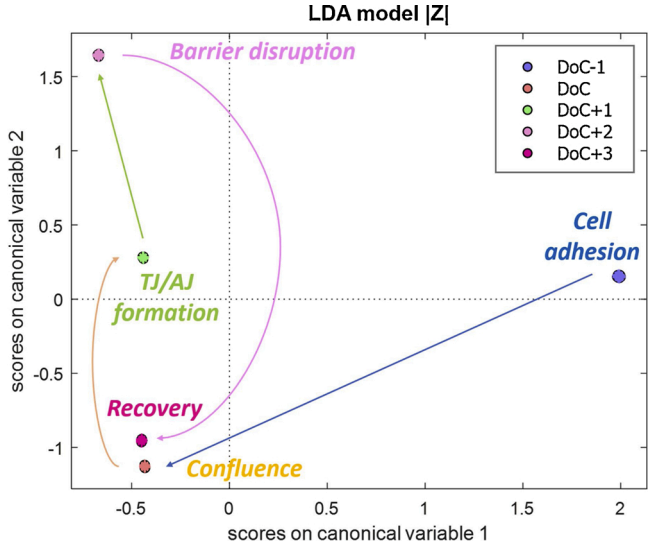

Fig. 7. LDA model based on impedance modulus |Z| with the selected set of features. Score plot on canonical variables 1-2.

the barrier is sensitive to ultrasounds which can be used for diagnostic purposes or to induce the barrier opening (BBBO) [35]. Regarding the DoC-1 class, the spectra show an evident resonance due to electrodes geometry and arrangement around 1.8 MHz in all the different intersections. This effect however is not present in the other classes so probably the confluent cells on top of the electrodes shift the resonance to a different frequency.

The classification results, resumed in Table 1, on the selected features have put also in evidence that it is possible to obtain almost perfect separation among the different time-points considering few frequencies as input features for the classification model. Interestingly, the model based on phase features is more sensitive to the feature selection with respect to the impedance-based model. This is something that could be subject to future investigations.

As a demonstration of the potentiality of the feature selection approach, we have shown one LDA model (Fig. 7), obtained using the measurements from 3 intersections for training and 2 for testing, exhibiting a complete separation between all the classes both in training and testing sets. In the first time-point of the experiment, cell confluency was very low, and the cells had not had enough time neither to generate a supporting extracellular matrix, nor to interact so much with neighboring cells. Therefore, this condition appeared as an isolated class (DoC-1). Then, the confluency condition was reached (DoC), the barrier matured progressively, starting to form junctional complexes (DoC+1) and finally the mannitol was administered, inducing a process of cell shrinking and vacuolation that ended up opening the barrier. This condition (DoC+2) results as well as an isolated cluster in the score plot, very distant from the other classes. After the treatment, cells started proliferating and re-constructing the barrier, going under a process of barrier recovery (DoC+3). The obtained barrier integrity level at DoC+3 was similar to the one observed at DoC, with high confluency of cells, although junctional complexes were not formed and therefore the barrier was still permeable. This similarity between DoC and DoC+3 observed in the classification model (Fig. 7) is coherent with the cell observation performed in the microscopy at each time-point (Supplementary Information Fig. S3).

The different barrier characteristics observed by the classification model performed, match the immunostaining results obtained. In μBBB-

controls, ZO-1 staining showed the formation of TJ both on the membrane-position and at the bottom-position (Fig. 3, a, b, e, f). VE-cadherin staining showed a poor staining at the bottom-position, and negative AJ signal at the membrane-position. At the membrane-position lower confluency levels (observed with nuclei staining), and lower ZO-1 expression, more localized on the nuclei, were detected. Previous reports suggested that ZO-1 localization in the cell is related to the maturity and extent of cell-cell contacts [36], being a nuclear localization at sub-confluency states representative of non-fully mature barriers, whereas peripheral plasma-membrane localization is an indicator of a mature barrier [36]. For the barrier formation and maturation, it was previously suggested that both AJ and TJ complex proteins have to interact during the barrier development [7,37]. Stable AJ, VE-cadherin in particular, are required for the EC survival, blood vessel assembly, stabilization and formation of TJ [37]. But at the same time, ZO-1 is essential for the VE-cadherin complex formation [7]. Furthermore, previous reports suggest that weakening of junctional complex proteins associated to VE-cadherin to form AJ, results in the activation of intracellular mechanisms to increase cell permeability [38].

After exposing cells seeded in μBBB devices to mannitol treatment (Fig. 3, c, d, g, h), cell confluency was severely affected specially at the bottom-position in samples or areas with only EC (Fig. 3, c–d and Supplementary Information Fig. S3 μBBB-EC-only device). ZO-1 expression became more nuclear and VE-cadherin expression vanished (Fig. 3, c, d, g, h). Although the barrier formed was not fully mature in the membrane-position or at the bottom-position of the device, these results suggest an active role of the pericytes in the integrity of the BBB and in the recovery from a hyperosmotic BBBO. The results are coherent with previous publications which evidenced the critical role of pericytes in the development, maintenance, and regulation of BBB [39,40]. Pericytes are not essential for the tightness of the BBB (e.g. they are not essential to induce TJ complex protein expression), but they are vital to avoid leakiness on the BBB by the regulation of the transcytosis of EC [27,28], the inhibition of immune cell trafficking and the permeation of agents that promote vascular permeability [41].

These results demonstrate that this method could be used to easily test membrane integrity under the effect of some compounds in real-time [42], or to monitor BBBO induced through drugs and to optimize specific pharmacological treatments. The platform and monitoring method, applied in this research for a study on the BBB, could be easily adapted for mimicking specific kind of blood vessels by changing the microchannel size, and it could be translated as well to mimic other biological barriers, such as blood-cerebrospinal fluid barrier, blood-spinal cord barrier, kidney glomerulus filtration barrier, etc. Translating the concept of TEER measurements to wideband impedance spectroscopy that we called Multi-frequency TEER (MTEER) enables not only to extract more information from a single experiment but also to investigate the frequency range that is most informative for the specific experimental conditions [43]. This method is also strengthened by its reliability. In fact, the accuracy values are relative to a massive amount of measurements and to a robust validation approach.

5. Conclusions

This work reports the use of wideband impedance spectroscopy for monitoring the BBB functionality exploiting machine learning algorithms. The measurements were performed across multiple positions in a frequency range up to tens of MHz, using a novel multi-layer microfluidic platform with integrated electrodes that can be fabricated with a rapid and cost-effective process.

To test this system, a simplified BBB model composed by EC and pericytes has been adopted. The cells were cultured inside the devices and the development of AJ and TJ has been observed. Administering mannitol resulted in an impairment of the barrier, affecting confluency of cells and the formation of junctional complexes. MTEER measurements, together with machine learning algorithms, resulted in an accurate technique to perform real-time non-invasive monitoring of the complex processes ongoing on the barrier, being able to distinguish through a multivariate representation the following phenomena occurring at different time-points: non-confluent cells, confluent monolayer, beginning of barrier sealing and junctional complexes formation, barrier opening after mannitol treatment, and its recovery. The results obtained through classification were confirmed with immunostainings.

The device and the analytic technique presented in this paper open a new path towards barrier systems monitoring that could easily be translated to studies of other biological barriers.

CRediT authorship contribution statement

Maider Badiola-Mateos: Conceptualization, Data curation, Investigation, Writing - original draft, Writing - review & editing. **Davide Di Giuseppe:** Conceptualization, Data curation, Investigation, Writing - original draft, Writing - review & editing. **Roberto Paoli:** Conceptualization, Data curation, Investigation, Writing - original draft, Writing - review & editing. **Maria Jose Lopez-Martinez:** Data curation, Writing - review & editing. **Arianna Mencattini:** Data curation, Writing - review & editing. **Josep Samitier:** Conceptualization, Project administration, Resources, Supervision, Writing - original draft, Writing - review & editing. **Eugenio Martinelli:** Conceptualization, Project administration, Resources, Supervision, Writing - original draft, Writing - review & editing.

Declaration of Competing Interest

There are no conflicts of interest to declare.

Acknowledgments

Authors want to acknowledge MicroFabSpace and Microscopy Characterization Facility, Unit 7 of ICTS “NANBIOSIS” from CIBER-BBN at IBEC. This work was supported by Networking Biomedical Research Center (CIBER), Spain. CIBER is an initiative funded by the VI National R&D&i Plan 2008–2011, Iniciativa Ingenio 2010, Consolider Program, CIBER Actions, and the Instituto de Salud Carlos III (RD16/0006/0012), with the support of the European Regional Development Fund. This work was funded by the CERCA Programme and by the Commission for Universities and Research of the Department of Innovation, Universities, and Enterprise of the Generalitat de Catalunya (2017 SGR 1079). This work has been developed in the context of AdvanceCat with the support of ACCIÓ (Catalonia Trade and Investment; Generalitat de Catalunya) under the Catalonian ERDF operational program (European Regional Development Fund) 2014–2020. This work was funded by the Spanish Ministry of Economy and Competitiveness (MINECO) through the projects MINDS (Proyectos I + D Excelencia + FEDER) TEC2015-70104-P, CTQ2016-75870-P, BIOBOT (Programa Explora Ciencia / Tecnología), TEC2015- 72718-EXP and RTI2018-097038-B-C21.

Appendix A. Supplementary data

Supplementary material related to this article can be found, in the online version, at doi:https://doi.org/10.1016/j.snb.2021.129599.

References

[1] C.R. Oliver, M.A. Altemus, T.M. Westerhof, H. Cheriyan, X. Cheng, M. Dziubinski, Z. Wu, J. Yates, A. Morikawa, J. Heth, M.G. Castro, B.M. Leung, S. Takayama, S. D. Merajver, A platform for artificial intelligence based identification of the extravasation potential of cancer cells into the brain metastatic niche, Lab Chip 19 (2019) 1162–1173, https://doi.org/10.1039/c8lc01387j.

[2] N.J. Abbott, A.A.K. Patabendige, D.E.M. Dolman, S.R. Yusof, D.J. Begley, Structure and function of the blood–brain barrier, Neurobiol. Dis. 37 (2010) 13–25, https://doi.org/10.1016/j.nbd.2009.07.030.

[3] N.J. Abbott, Blood–brain barrier structure and function and the challenges for CNS drug delivery, J. Inherit. Metab. Dis. 36 (2013) 437–449, https://doi.org/10.1007/s10545-013-9608-0.
[4] S.M. Stamatovic, A.M. Johnson, R.F. Keep, A.V. Andjelkovic, Junctional proteins of the blood-brain barrier: new insights into function and dysfunction, Tissue Barriers 4 (2016), e1154641, https://doi.org/10.1080/21688370.2016.1154641.
[5] R.F. Keep, A.V. Andjelkovic, J. Xiang, S.M. Stamatovic, D.A. Antonetti, Y. Hua, G. Xi, Brain endothelial cell junctions after cerebral hemorrhage: changes, mechanisms and therapeutic targets, J. Cereb. Blood Flow Metab. 38 (2018) 1255–1275, https://doi.org/10.1177/0271678X18774666.
[6] W. Li, Z. Chen, I. Chin, Z. Chen, H. Dai, The role of VE-cadherin in blood-brain barrier integrity under central nervous system pathological conditions, Curr. Neuropharmacol. 16 (2018) 1375–1384, https://doi.org/10.2174/1570159X16666180222164809.
[7] O. Tornavaca, M. Chia, N. Dufton, L.O. Almagro, D.E. Conway, A.M. Randi, M. A. Schwartz, K. Matter, M.S. Balda, ZO-1 controls endothelial adherens junctions, cell–cell tension, angiogenesis, and barrier formation, J. Cell Biol. 208 (2015) 821–838, https://doi.org/10.1083/jcb.201404140.
[8] N.R. Saunders, K.M. Dziegielewska, K. Møllgård, M.D. Habgood, Markers for blood-brain barrier integrity: how appropriate is Evans blue in the twenty-first century and what are the alternatives? Front. Neurosci. 9 (2015) 1–16, https://doi.org/10.3389/fnins.2015.00385.
[9] B. Srinivasan, A.R. Kolli, M.B. Esch, H.E. Abaci, M.L. Shuler, J.J. Hickman, TEER measurement techniques for in vitro barrier model systems, J. Lab. Autom. 20 (2015) 107–126, https://doi.org/10.1177/2211068214561025.
[10] M.W. van der Helm, O.Y.F. Henry, A. Bein, T. Hamkins-Indik, M.J. Cronce, W. D. Leineweber, M. Odijk, A.D. van der Meer, J.C.T. Eijkel, D.E. Ingber, Non-invasive sensing of transepithelial barrier function and tissue differentiation in organs-on-chips using impedance spectroscopy, Lab Chip 19 (2019) 452–463, https://doi.org/10.1039/c8lc00129d.
[11] C.G. Jones, C. Chen, An arduino-based sensor to measure transendothelial electrical resistance, Sensors Actuators A Phys. 314 (2020), 112216, https://doi.org/10.1016/j.sna.2020.112216.
[12] A. Kincses, A.R. Santa-Maria, F.R. Walter, L. Dér, N. Horányi, D.V. Lipka, S. Valkai, M.A. Deli, A. Dér, A chip device to determine surface charge properties of confluent cell monolayers by measuring streaming potential, Lab Chip 20 (2020) 3792–3805, https://doi.org/10.1039/d0lc00558d.
[13] K. Benson, S. Cramer, H.J. Galla, Impedance-based cell monitoring: barrier properties and beyond, Fluids Barriers CNS 10 (2013) 1–11, https://doi.org/10.1186/2045-8118-10-5.
[14] A.R. Santa-Maria, F.R. Walter, S. Valkai, A.R. Brás, M. Mészáros, A. Kincses, A. Klepe, D. Gaspar, M.A.R.B. Castanho, L. Zimányi, A. Dér, M.A. Deli, Lidocaine turns the surface charge of biological membranes more positive and changes the permeability of blood-brain barrier culture models, Biochim. Biophys. Acta Biomembr. 1861 (2019) 1579–1591, https://doi.org/10.1016/j.bbamem.2019.07.008.
[15] J. Yeste, X. Illa, M. Alvarez, R. Villa, Engineering and monitoring cellular barrier models, J. Biol. Eng. 12 (2018) 18, https://doi.org/10.1186/s13036-018-0108-5.
[16] A. Oddo, B. Peng, Z. Tong, Y. Wei, W.Y. Tong, H. Thissen, N.H. Voelcker, Advances in microfluidic blood–brain barrier (BBB) models, Trends Biotechnol. 37 (2019) 1295–1314, https://doi.org/10.1016/j.tibtech.2019.04.006.
[17] S. Jeong, S. Kim, J. Buonocore, J. Park, C.J. Welsh, J. Li, A. Han, A three-dimensional arrayed microfluidic blood–brain barrier model with integrated electrical sensor array, IEEE Trans. Biomed. Eng. 65 (2018) 431–439, https://doi.org/10.1109/TBME.2017.2773463.
[18] B.M. Maoz, A. Herland, O.Y.F. Henry, W.D. Leineweber, M. Yadid, J. Doyle, R. Mannix, V.J. Kujala, E.A. FitzGerald, K.K. Parker, D.E. Ingber, Organs-on-Chips with combined multi-electrode array and transepithelial electrical resistance measurement capabilities, Lab Chip 17 (2017) 2294–2302, https://doi.org/10.1039/C7LC00412E.
[19] F.R. Walter, S. Valkai, A. Kincses, A. Petneházi, T. Czeller, S. Veszelka, P. Ormos, M.A. Deli, A. Dér, A versatile lab-on-a-chip tool for modeling biological barriers, Sensors Actuators B Chem. 222 (2016) 1209–1219, https://doi.org/10.1016/j.snb.2015.07.110.
[20] D. Ren, C.O. Chui, Feasibility of tracking multiple single-cell properties with impedance spectroscopy, ACS Sens. 3 (2018) 1005–1015, https://doi.org/10.1021/acssensors.8b00152.
[21] https://www.wpi-europe.com/products/cell-and-tissue/teer-measurement/evom3.aspx, (n.d.).
[22] T. Gerasimenko, S. Nikulin, G. Zakharova, A. Poloznikov, V. Petrov, A. Baranova, A. Tonevitsky, Impedance spectroscopy as a tool for monitoring performance in 3D models of epithelial tissues, Front. Bioeng. Biotechnol. 7 (2020), https://doi.org/10.3389/fbioe.2019.00474.
[23] P.S. Nunes, P.D. Ohlsson, O. Ordeig, J.P. Kutter, Cyclic olefin polymers: emerging materials for lab-on-a-chip applications, Microfluid. Nanofluidics 9 (2010) 145–161, https://doi.org/10.1007/s10404-010-0605-4.
[24] A. Piruska, I. Nikcevic, S.H. Lee, C. Ahn, W.R. Heineman, P.A. Limbach, C. J. Seliskar, The autofluorescence of plastic materials and chips measured under laser irradiation, Lab Chip 5 (2005) 1348, https://doi.org/10.1039/b508288a.
[25] A. Liga, J.A.S. Morton, M. Kersaudy-Kerhoas, Safe and cost-effective rapid-prototyping of multilayer PMMA microfluidic devices, Microfluid. Nanofluidics 20 (2016) 164, https://doi.org/10.1007/s10404-016-1823-1.
[26] R. Booth, H. Kim, Characterization of a microfluidic in vitro model of the blood-brain barrier (μBBB), Lab Chip 12 (2012) 1784, https://doi.org/10.1039/c2lc40094d.
[27] A. Armulik, G. Genové, M. Mäe, M.H. Nisancioglu, E. Wallgard, C. Niaudet, L. He, J. Norlin, P. Lindblom, K. Strittmatter, B.R. Johansson, C. Betsholtz, Pericytes regulate the blood-brain barrier, Nature 468 (2010) 557–561, https://doi.org/10.1038/nature09522.
[28] R. Daneman, L. Zhou, A.A. Kebede, B.A. Barres, Pericytes are required for blood–brain barrier integrity during embryogenesis, Nature 468 (2010) 562–566, https://doi.org/10.1038/nature09513.
[29] A. Herland, A.D. van der Meer, E.A. FitzGerald, T.-E. Park, J.J.F. Sleeboom, D. E. Ingber, Distinct contributions of astrocytes and pericytes to neuroinflammation identified in a 3D human blood-brain barrier on a chip, PLoS One 11 (2016), e0150360, https://doi.org/10.1371/journal.pone.0150360.
[30] R. Cecchelli, S. Aday, E. Sevin, C. Almeida, M. Culot, L. Dehouck, C. Coisne, B. Engelhardt, M.P. Dehouck, L. Ferreira, A stable and reproducible human blood-brain barrier model derived from hematopoietic stem cells, PLoS One 9 (2014), e99733, https://doi.org/10.1371/journal.pone.0099733.
[31] Impedance Measurement Handbook, Keysight Technologies, Agilent, 2009, p. 140. www.keysight.com.
[32] M. Jordan, J. Kleinberg, B. Schölkopf, Pattern Recognition and Machine Learning, 1st ed., Springer-Verlag, New York, New York, 2006.
[33] D. Ballabio, V. Consonni, Classification tools in chemistry. Part 1: linear models, PLS-DA Anal. Methods 5 (2013) 3790, https://doi.org/10.1039/c3ay40582f.
[34] G. Zhang, R. Zhu, Effect of parasitic capacitance on impedance measurement and model extraction, Electroanalysis 22 (2010) 351–358, https://doi.org/10.1002/elan.200900324.
[35] K.F. Bing, G.P. Howles, Y. Qi, M.L. Palmeri, K.R. Nightingale, Blood-brain barrier (BBB) disruption using a diagnostic ultrasound scanner and definity® in mice, Ultrasound Med. Biol. 35 (2009) 1298–1308, https://doi.org/10.1016/j.ultrasmedbio.2009.03.012.
[36] C.J. Gottardi, M. Arpin, A.S. Fanning, D. Louvard, The junction-associated protein, zonula occludens-1, localizes to the nucleus before the maturation and during the remodeling of cell-cell contacts, Proc. Natl. Acad. Sci. 93 (1996) 10779–10784, https://doi.org/10.1073/pnas.93.20.10779.
[37] S. Tietz, B. Engelhardt, Brain barriers: crosstalk between complex tight junctions and adherens junctions, J. Cell Biol. 209 (2015) 493–506, https://doi.org/10.1083/jcb.201412147.
[38] M. Giannotta, M. Trani, E. Dejana, VE-cadherin and endothelial adherens junctions: active guardians of vascular integrity, Dev. Cell 26 (2013) 441–454, https://doi.org/10.1016/j.devcel.2013.08.020.
[39] C.-H. Lai, K.-H. Kuo, The critical component to establish in vitro BBB model: pericyte, Brain Res. Rev. 50 (2005) 258–265, https://doi.org/10.1016/j.brainresrev.2005.07.004.
[40] M. Blanchette, R. Daneman, Formation and maintenance of the BBB, Mech. Dev. 138 (2015) 8–16, https://doi.org/10.1016/j.mod.2015.07.007.
[41] R.P. Moura, A. Almeida, B. Sarmento, The role of non-endothelial cells on the penetration of nanoparticles through the blood brain barrier, Prog. Neurobiol. 159 (2017) 39–49, https://doi.org/10.1016/j.pneurobio.2017.09.001.
[42] K. Shigetomi, Y. Ono, T. Inai, J. Ikenouchi, Adherens junctions influence tight junction formation via changes in membrane lipid composition, J. Cell Biol. 217 (2018) 2373–2381, https://doi.org/10.1083/jcb.201711042.
[43] J. Wegener, C.R. Keese, I. Giaever, Electric cell-substrate impedance sensing (ECIS) as a noninvasive means to monitor the kinetics of cell spreading to artificial surfaces, Exp. Cell Res. 259 (2000) 158–166, https://doi.org/10.1006/excr.2000.4919.

Maider Badiola-Mateos is a Ph.D. student at the Department of Electronics and Biomedical Engineering of University of Barcelona. Her research interests are related to the 3D in-vitro modelling of the neuromuscular circuit and on its application in the development of pharmacological treatments for neurodegenerative diseases.

Davide Di Giuseppe is a Postdoctoral Researcher at the Department of Electronic Engineering of University of Rome Tor Vergata. In 2020 he received the Ph.D. degree in Engineering of Sensorial and Learning Systems from University of Rome Tor Vergata. His research is focused on the development of automated sensorial systems for biomedical applications based on Lab-On-Chip and live cell microscopy. His technical skills include electronic circuit design, microfabrication, photolithography, mechanical prototyping and microfluidics.

Roberto Paoli received the Ph.D. degree in Biomedicine from University of Barcelona in 2019. His research is related to the microfabrication of cell culture interfaces for organ-on-chip applications.

Maria José López-Martinez is a Senior Researcher at IBEC since 2016. PhD on the design and fabrication of micro/nano tools to be applied in life sciences (IMB-CNM, CSIC). She performed several postdoctoral stays focusing her work in developing microfluidics devices for biomedical applications, particularly she was working at University of Groningen, University of Hull and INESC MN. Her current research lines are focused in the use of microfabrication, micromachining and 3D technologies to understand how functional units of organs work to improve medical diagnostics and therapies. Specifically, she is involved in different projects using Lab-on-a-Chip (LoC) and organ-on-chips (OoC) technologies to emulate spleen and blood-brain barrier.

Arianna Mencattini is an Assistant Professor at the Department of Electronic Engineering, University of Rome Tor Vergata. Her main research interests are related to image and video processing techniques for the development of computed assisted diagnosis systems,

analysis of speech and facial expressions for the automatic emotion recognition, and for the design of novel cell analysis algorithms for biological investigations. She has co-authored more than 100 papers on international journal and conferences and she co-edited two books on computerized medical diagnosis.

Josep Samitier is Director of the Institute for Bioengineering of Catalonia (IBEC) and Full Professor in the Physics Faculty (Electronic Dep.), University of Barcelona. From February 1984 to June 1985 he was visiting research fellow at the Philips Electronic Laboratory, Paris, France. From March 2001 to June 2005 Prof. Samitier was Deputy Head of the Barcelona Science Park (PCB), and in 2003 he received the Barcelona city Prize of the Barcelona Council in the area of technology. Prof. Samitier is the coordinator of the Spanish Platform on Nanomedicine and the president of the Associació Catalana d'Entitats de Recerca (ACER).

Eugenio Martinelli is an Associate Professor at the Department of Electronic Engineering of the University of Rome Tor Vergata where he teaches courses on fundamentals of electronics, Sensors and Pattern Recognition. His research activity is mainly focused on the development of sensors and their interface, lab-on-chip, and pattern recognition algorithms for medical and space applications. He authored more than 200 papers on international journals and conference proceedings. He was member of the organizing committee of national and international conferences in sensors.